JOURNAL OF AIRCRAFT
Vol. 33, No. 2, March–April 1996

Measurements and Visualization in the Flowfield Behind a Model Propeller

Ryuji Fukada*
Nissan Motor Company, Ltd., Kanagawa 243-01, Japan
Hani Nigim†
Birzeit University, Birzeit, Israel
and
Hide Koyama‡
Tokyo Denki University, Tokyo 101, Japan

An experimental investigation of the flowfield behind a two-bladed propeller was conducted by using both smoke-wire flow visualization and hot-wire anemometer techniques. The mean-time and the ensemble-averaged distributions and velocity unsteadiness data were obtained. The results revealed the tip–vortex formation mechanism and the reverse flow in the outer region of the flowfield as well as a strong defect in the flow directly behind the blades. High unsteadiness was found within the blade wake, while much lower values were observed with the increasing distance downstream of the wake region. Also, the transformation of the core-flow from a jet-like to a wake-like flow and the influences of hub–vortex shedding into the wake were reported.

Nomenclature

C = blade code
n = number of revolutions
R = propeller tip radius
V = velocity
X, Y, Z = coordinates
ϕ = circumferential position

Subscripts
m = time mean
x = radial
y = tangential
z = axial

Introduction

RECENT studies have shown that propeller aircraft offer a fuel-efficient propulsion for the near future. Therefore, considerable interest has focused on the development of new and advanced propeller concepts. However, the impact of these concepts on the flowfield in the immediate vicinity of the propeller raises a number of important engineering issues of concern, such as propeller/body interaction, noise generation, vibrations, and control surface effectiveness.

Although the aerodynamics of propellers have been the subject of study for many years, most of the experimental work has been concentrated on blade design, whereas the theoretical work is usually based on simple modeling approaches of vortex theory.[1] To analyze the flow behind an aircraft propeller it is necessary to have more accurate modeling. Chang et al.[2] and Kobayakawa et al.[3] presented interesting results for swept blades using the vortex–lattice method and nonlinear programming. Mastsuo et al.[4] employed time-averaged Navier–Stokes equations to model the flow around the propeller. The effect of vortex core distortion on blade–vortex interaction was analyzed for two-dimensional, incompressible, inviscid flow.[5–7] In all reported analysis, assumptions of tip–vortex geometry and the rate of contraction of the wake were required.

A number of experimental works have been done on the flow behind the propeller to validate the usability of laser Doppler velocimeter (LDV) and its data acquisition system.[8–10] Lepicovsky et al.[8] and Lepicovsky[9] carried out a relatively simple experiment to measure the flowfield of a two-bladed propeller using LDV to verify their data reduction procedure. Murthy et al.[10] reported mean flow measurements in the end-wall region of a compressor rotor. Most recently, the near-field behavior of a tip-vortex, as well as the three-dimensional characteristics of a propeller wake were studied.[11–13]

The primary objective of the experimental work presented in this article is to obtain a better understanding of the occurrence and behavior of the tip–vortex geometry. Also, to study the wake behind a nonflight propeller and to investigate the complex velocity flowfields about the propeller. An additional objective of this work is to build a database that could be used for validation of the analytical and the numerical modeling codes. Two measurement techniques with varying levels of sophistication and accuracy were applied throughout this work. The first was smoke-wire flow visualization, and the second technique was based on a hot-wire anemometer. To avoid the compressibility effects, the blade-tip Mach number was maintained below 0.1.

Apparatus and Instrumentation

The two-bladed propeller model (LMK Co., no. 16-7.5) used in this experiment is manufactured for radio-controlled airplanes. The propeller diameter is 406 mm and is made of plastic. The apparatus and the propeller dimensions together with cross-sectional profiles of the propeller blade are given in Fig. 1. The propeller was driven by an ac servomotor (Yaskawa Electric Manufacturing Co., Ltd., USAHEM-03AB) through a transmission and shaft system. During the present work, the propeller was run at a rotating speed of 1500 rpm. The corresponding blade-tip velocity was 31.9 m/s and the tip Mach number was less than 0.1. A rotary encoder (Omron Co., E6B),

Received March 13, 1994; revision received Oct. 10, 1995; accepted for publication Nov. 20, 1995.

*Specialist Engineer.
†Associate Professor, Department of Mechanical Engineering, P.O. Box 14. Associate Fellow AIAA.
‡Professor, Department of Mechanical Engineering.

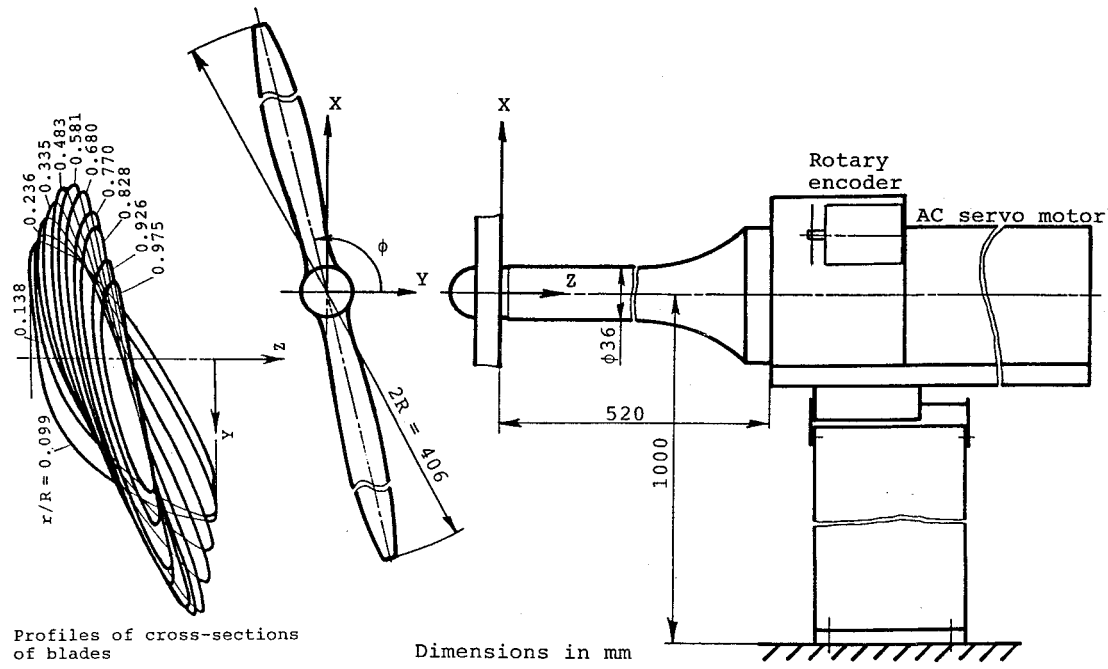

Fig. 1 Propeller rotating testing facility.

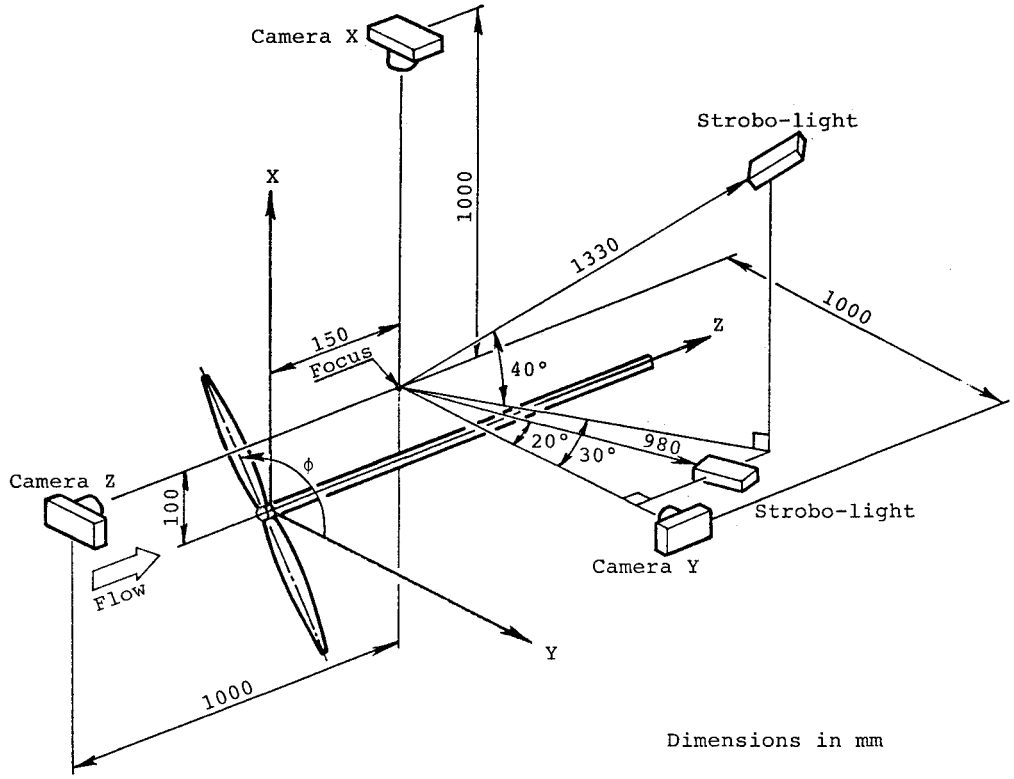

Fig. 2 Three-dimensional flow visualization arrangement and coordinate system.

which gave a two-phase output of 1 and 360 pulses/rev, operating at the same rotating speed as the propeller shaft, was installed to obtain the required angular position of the propeller. To avoid disturbing the incoming flow, the running engine and the propeller boss were covered by a nacelle and spinner, respectively. In the present experiment, however, a slender propeller shaft 520 mm in length and 36 mm in diameter was used to measure the effect of the nacelle on the flowfield behind the propeller.

A smoke-wire method of flow visualization was used to reveal the tip–vortex patterns and the flowfield behind the propeller. A nichrome wire of 0.1 mm in diameter was kinked by passing it through the teeth of two cogwheels of the module equal to 0.5. The kinked wire of about 400 mm length was stretched vertically in the immediate vicinity of the propeller, at location Z, equaling 3 mm from the back of the propeller. Then the wire was painted with a mixture of paraffin liquid and aluminum powder. A dense white smoke was produced by passing a strong current through the wire. The flowfield was examined by taking instantaneous photographs of the smoke streaklines from the top, front, and side views using three cameras located at each position and two stroboscope lights. The

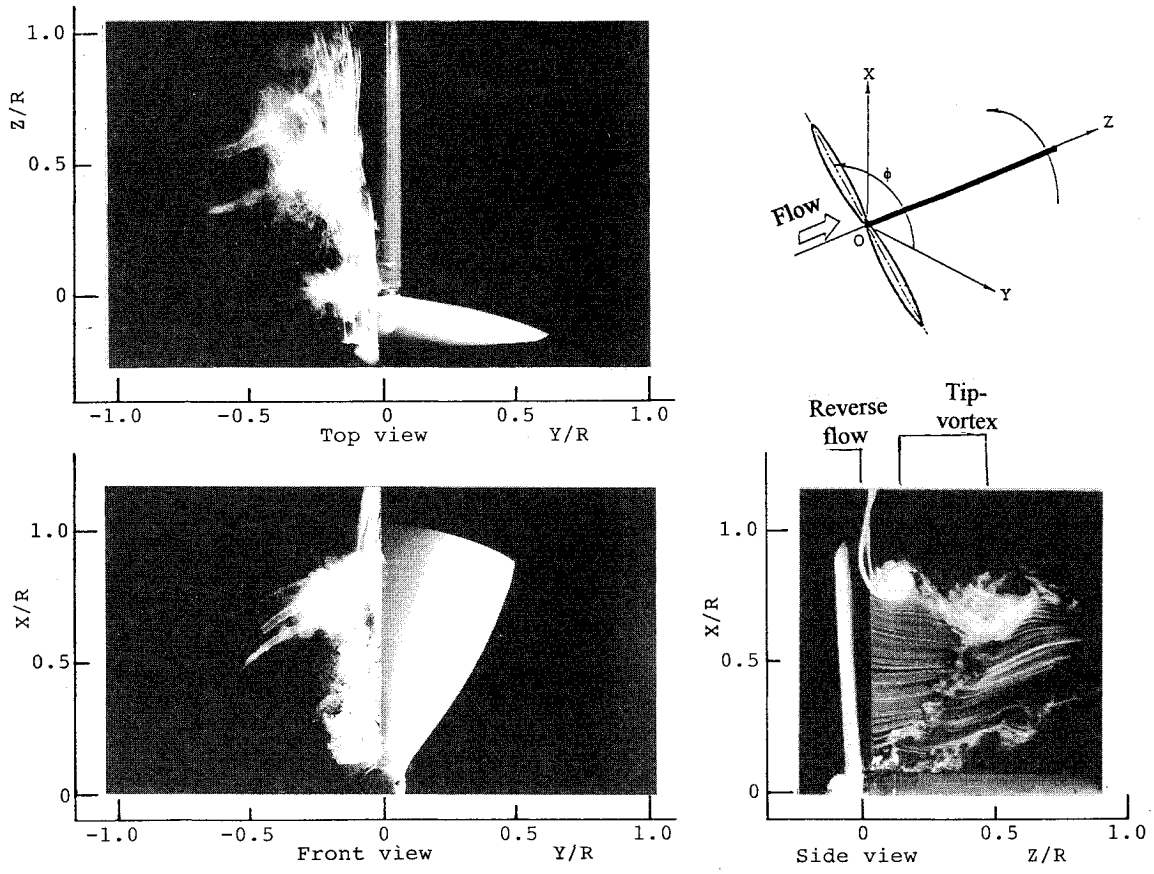

Fig. 3 Photographs of instantaneous smoke-streakline patterns behind rotating propeller; n = 1500 rpm and ϕ = 790 deg.

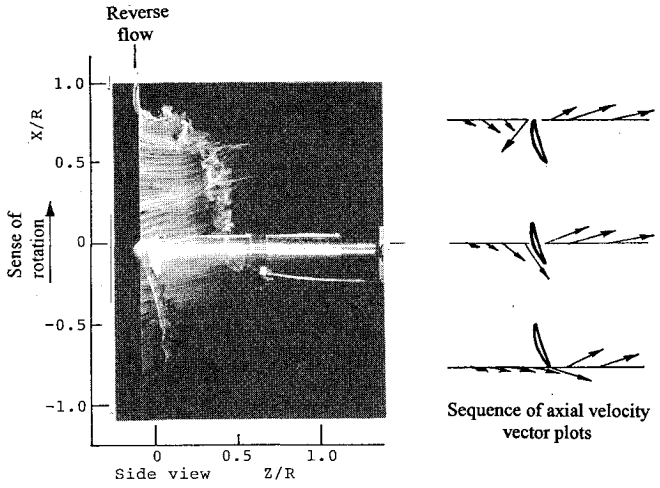

Fig. 4 Photograph of instantaneous smoke-streakline patterns at dimensionless radius of 0.5; propeller at horizontal position ϕ = 720 deg.

three-dimensional flow arrangement and coordinate system are shown in Fig. 2. The focus of the cameras was positioned at the point of X = 100 mm, Y = 0.0 mm, and Z = 150 mm. The shutter of the cameras was released by the rotary encoder system. An electronic circuit to control the timing of the generation of smoke and the flash illumination at a required angular position of the propeller was designed. When the propeller was at the vertical position, the dense white smoke was generated. For each set of experimental data, photographs were taken for two complete revolutions of the shaft with a 10-deg interval, i.e., 216 photographs. To ensure durability of the data, each experiment was repeated twice, and if disagreement was reported a third set was obtained.

A hot-wire anemometer (Dantex Elektronik, 56N16 and 56N21), having a 5-μm tungsten slanted wire mounted at 45 deg to the probe axis, was used for the measurements of the mean-time and the ensemble-averaged (blade-to-blade) distributions, as well as velocity unsteadiness data for three of the velocity components in the flowfield. At a particular point, the hot-wire readings were taken from three different wire orientations. Then, the determination of the three velocity components was obtained from sums and differences of the voltage recorded by the hot wire and from the calibration velocity vs an output–voltage relationship. This measurement technique, together with flow visualization data, allows the determination of the direction of the velocity in relation with the azimuthal displacement of the blade. The hot-wire data were obtained, at given radial stations of 1-deg-angular intervals, in the form of pulses controlled by the rotary encoder, 360 pulses/rev.

To yield accurate time-averaged quantities, the raw data were acquired and saved over a sufficient period of time; the data were averaged for a systematically varying number of sweeps. At each measuring position, at least 200 sampling values of the dc signal were passed to the computer (Nec Co., PC-9801), where the mean and the ensemble-averaged velocity distributions were computed. The velocity unsteadiness was computed as a rms standard deviation of the local velocity fluctuations normalized by the local ensemble-averaged velocity. Using the analysis of Ref. 14, the error in the mean flow velocity measurement, for a confidence level of 95%, was estimated to be about 3% in the higher turbulence region.

Experimental Results

A large amount of flow visualization and hot-wire anemometer data were obtained for the propeller running at 1500 rpm at nonflight (static) conditions. The visualization helps to explain, qualitatively, the wake behavior of the propeller blade. The hot-wire data indicate the influence of the tip–vortex,

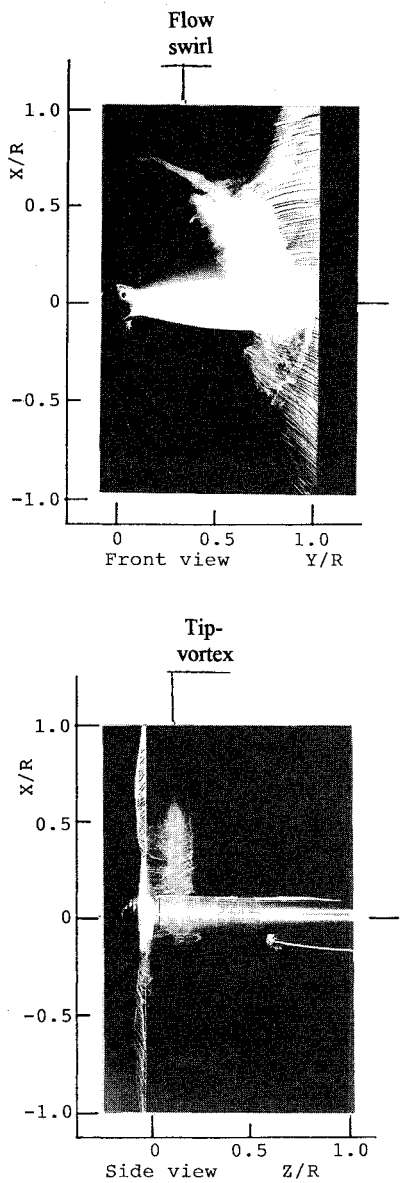

Fig. 5 Photographs of instantaneous smoke-streaklines patterns around blade tip; propeller at ϕ = 720 deg.

hub–vortex, and reverse flows on the three velocity components. Top, front, and side-view photographs of the instantaneous smoke-streakline patterns around the rotating propeller at an angular position equal to 790 deg are shown in Fig. 3. In the side-view photographs, both the reverse flow and the tip–vortex are clearly visible. The cores of the tip–vortex are visible in the front-view photographs. Immediately after the blade passed the X–Z plane, a reversed flow was formed around the blade tip and became a tip–vortex in which swirl direction was counterclockwise. The distortion of the core-flow, and its transformation from jet-like to wake-like flow is seen together with hub–vortex shedding into the wake. Because of the small relative velocity of the fluid in the blade wake, the absolute velocity of the fluid in the wake has a different flow direction from the rest of the fluid outside the wake, thus, generating the propeller flow swirl.

From the analysis of many similar sets of photographs, the regions of reversed flow at the blade tip are developed along the blade height from the undisturbed freestream at about $1.2X/R$, to the tip–vortex region at about $0.8X/R$, where X is a vertical distance from the propeller center and R is the propeller tip radius. Based on the inspection of those photographs, it is clear that the tip–vortex is distorted toward the blade and leads to large aerodynamic interference effects when the tip–vortex of one blade passes close to the following blade. Figure 3 shows the complex three-dimensional flowfield behind the propeller and the transformation of the jet-like flow to wake-like flow in the core-flow region.

To observe changes in the flowfield caused by the blade-induced local flow, a smoke wire was stretched vertically in the immediate vicinity of the propeller front at a dimensionless radius of Y/R = 0.50. The side-view photograph together with the flow vector plots, as generated at the axial station, are shown in Fig. 4. In this figure, the propeller is positioned horizontally. A diagonal line composed of the inclined smoke-streaklines is observed on the trailing side of the blade. In addition, an oscillating wake is also observed downstream of the trailing edge. With the assistance of the flow vector, a close look at Fig. 4 reveals that, in the region just in front of the propeller disc, the flow starts to turn against the propeller motion and even reverses in the axial direction in the region close to the stagnation point on the blade surface. As the blade leaves the line of measurements, a large velocity increase is observed at the trailing edge.

To have a better understanding of the formation mechanism and the growth of the tip–vortex, the flowfield about the blade tip of the propeller was visualized by using a smoke wire

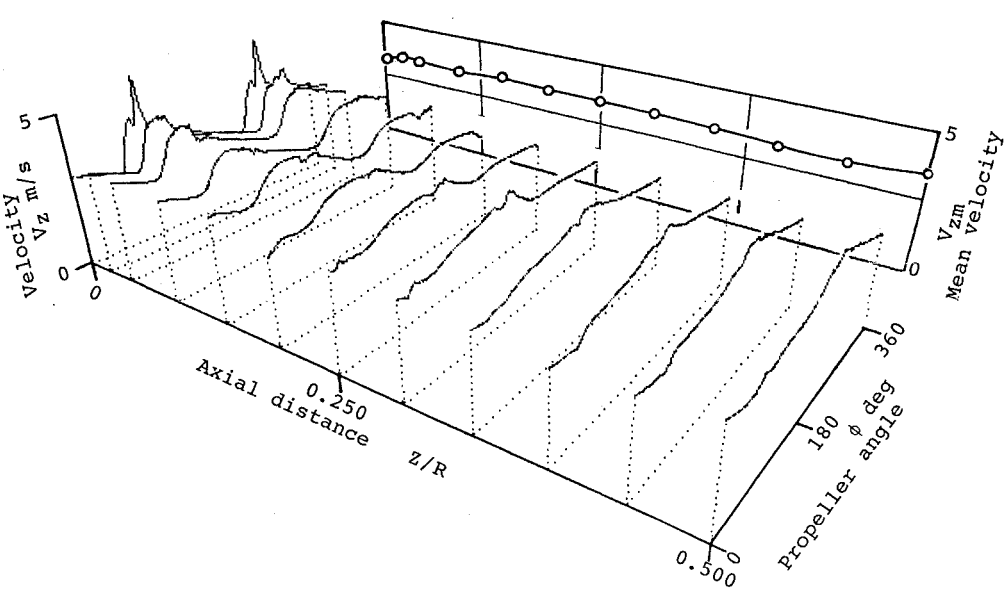

Fig. 6 Axial distributions of ensemble-averaged velocity field behind propeller; Y/R = 0.517 and n = 1500 rpm.

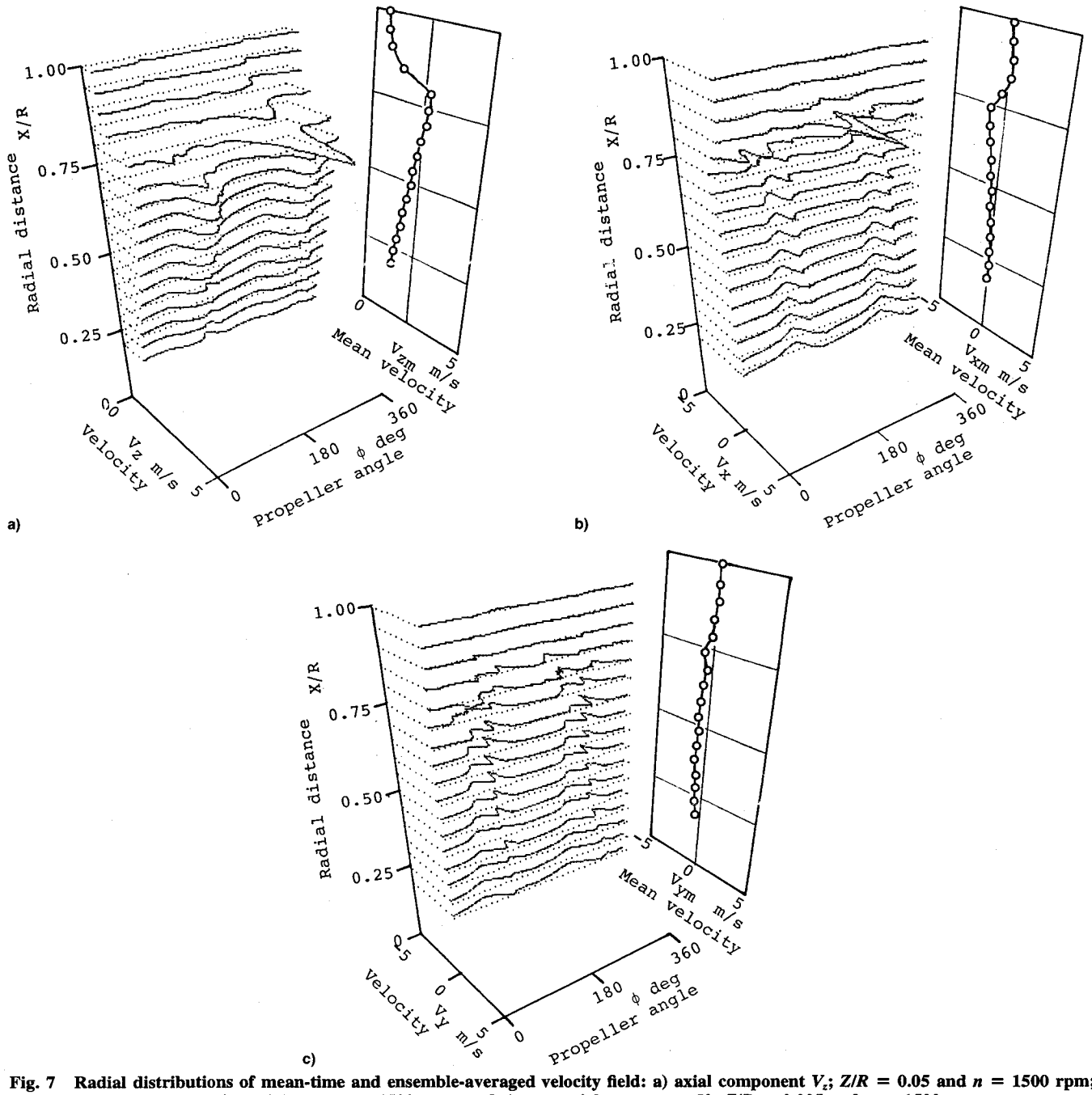

Fig. 7 Radial distributions of mean-time and ensemble-averaged velocity field: a) axial component V_z; Z/R = 0.05 and n = 1500 rpm; b) radial component V_x; Z/R = 0.05 and n = 1500 rpm; and c) tangential component V_y; Z/R = 0.025 and n = 1500 rpm.

stretched vertically near the blade tip. The focus of the cameras in the flow visualization arrangement (see Fig. 2) was positioned at the point of $X = 0.0$ mm, $Y = 203$ mm, and $Z = -7.5$ mm. Figure 5 shows the front and side-view photographs of the flow pattern about the blade tip of the propeller that is in a horizontal position. The core of the tip–vortex of the preceding blade is observed in the vicinity of the propeller disc, as well as a small core of the tip–vortex of the following blade at the trailing edge of the blade tip. Reverse flow across the blade tip from the leading surface to the trailing surface is clearly visible in the side-view photograph.

The blade-to-blade distributions of the axial velocity components behind the rotating propeller are illustrated in Fig. 6. The measurements were carried out at $Y/R = 0.517$, which is in the core-flow region behind the propeller and away from the tip or the hub effects. As in Ref. 9, the mean velocity distribution is plotted on the background grid, while the blade-to-blade distributions are shown in the front of the plot. The ensemble-averaged distributions agree with the mean velocity data. It is clear from Fig. 6 that the mean velocity measurements are not enough to represent the flow behavior behind a rotating propeller, because ensemble blade-to-blade distributions disclose a considerable nonuniformity of the measured velocity in the circumferential direction.

The ensemble-averaged axial, radial, and tangential velocity components, for a location just behind the propeller, at Z/R = 0.05, are shown in Figs. 7a–7c, together with corresponding mean velocity distributions. The figures demonstrate interesting features of the flowfield in both the reverse flow and tip–vortex regions. In these regions, while both axial velocity and radial velocity components show violent velocity fluctuations (Figs. 7a and 7b), the tangential velocity component, which in fact defines the swirl of the slipstream, is mildly affected (Fig. 7c). These results are confirming the flow visualization that are data given in Fig. 3. The maximum axial velocity component is located at about $X/R = 0.8$ and starts to gradually decrease.

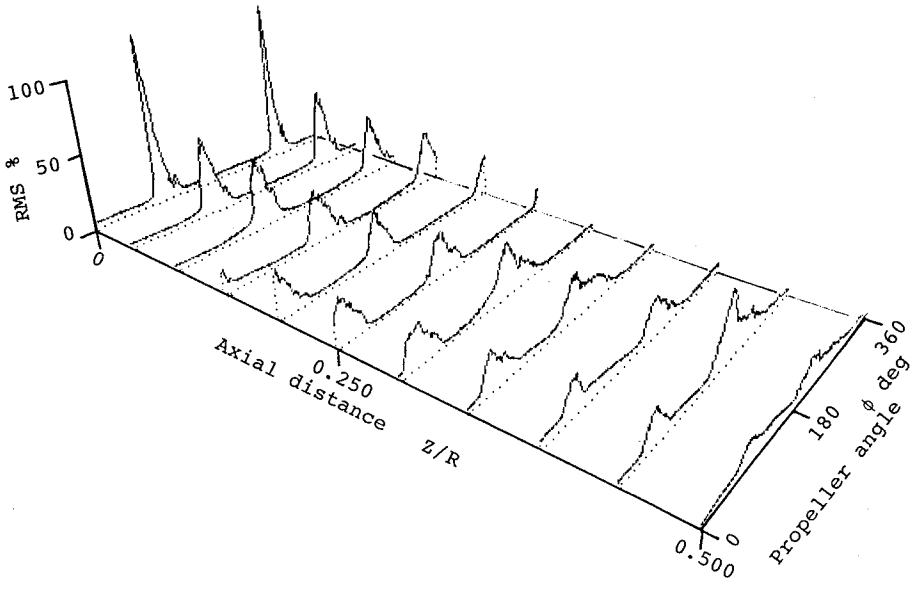

Fig. 8 Axial velocity unsteadiness profiles behind propeller; at X/R = 0.517 and n = 1500 rpm.

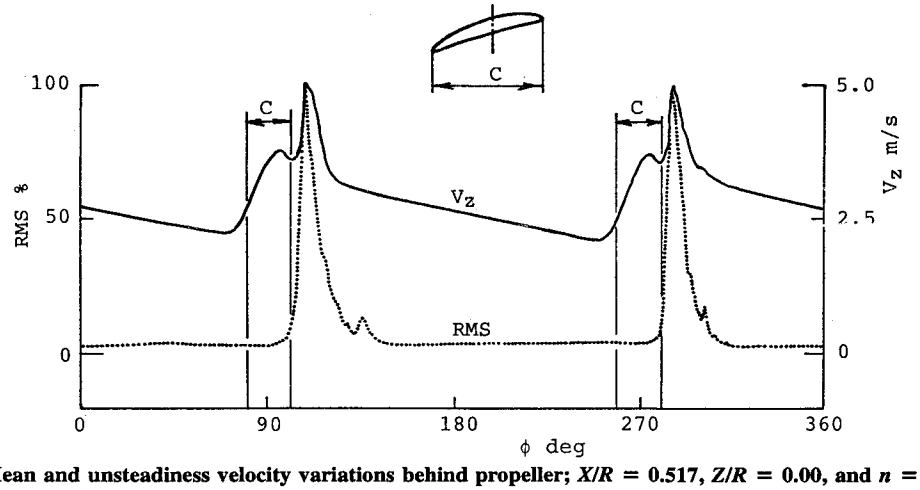

Fig. 9 Mean and unsteadiness velocity variations behind propeller; X/R = 0.517, Z/R = 0.00, and n = 1500 rpm.

Also, the radial velocity component reaches its largest magnitude in the reverse direction in the region of the flow separation at the blade tip close to the propeller.

At a particular dimensionless radius of X/R = 0.517, the axial blade-to-blade distributions of velocity unsteadiness are obtained and plotted against the propeller circumferential position in Fig. 8. The measured data show that just behind the propeller, a high-velocity unsteadiness drops rapidly towards moderate values with increasing distance from the propeller. The figure confirms the three-dimensional character of the flowfield because of the propeller blade wake.

Velocity variations along an angular station, which is fixed with respect to the rotating propeller and facing the pressure side (lower surface) of the blades at X/R = 0.517, were measured. In Fig. 9, the data are plotted against the angular position. The axial mean velocity is rapidly accelerated by blade and wake impact in the direction of the blade rotation. Also, a visible unsteadiness of the velocity can be seen within the blade chord wake region. All variations and higher values of mean and unsteadiness velocities are confined within the blade chord region, which could be used as an indication of the associated vortex sheet distribution. This vortex sheet is, in fact, a shear layer within which there is a very steep velocity gradient. Also in the figure, the unsteadiness of the vortex sheet emanating from the upper surface of the blade trailing edge was clearly observed. Higher unsteadiness was found within the blade wake regions.

The present work offers a unique opportunity to compare the hot-wire data with those reported in Lepicovesky,[9] where a similar investigation was made using a laser velocimeter technique. The agreement between the axial velocity distribution is good, except for the region behind the propeller. The striking difference is that, in the present work, sharp velocity defects indicating the presence of viscous wake is generated behind the propeller disc. This discrepancy may be because of the large mixing that was observed in that region. Thus, the presence of the hot-wire probe would affect the flowfield. The effect is most pronounced in phenomena whose length scale is smaller than the probe size. Other inaccuracies associated with hot wire are the directional and spatial errors.

In the experimental setup of Lepicovesky,[9] the fluid in the region immediately behind the propeller was poorly seeded. This was partially because of the fact that the particles diameter was of seeding oil below the required minimum value recommended for such measurement. Hence, the noise-to-signal ratio is high, which makes the validity of the LDV measurement in the region immediately behind the propeller disc also questionable.

Finally, the agreement between the axial and unsteadiness velocities, acquired from the LDV system and the hot-wire probe downstream of the trailing edge of the rotating blade, is excellent. The previous comparisons provide validation of the present as well as earlier data.

Conclusions

Two experimental techniques were used to study the three-dimensional flowfield behind a rotating propeller. The smoke-wire visualization method appears to be suitable for obtaining detailed information about the reverse, tip–vortex, core flow, and hub–vortex regions. The hot-wire measurement technique is still good enough to carry out blade-to-blade studies in the complex flowfield.

Immediately behind the rotating propeller, the tip–vortex shedding is in the form of a helical line vortex streaming from the tip of each blade, while the hub vortex is shed into the wake so that the bound circulation falls to zero at the hub–blade position. Also, sheet vortex was observed in the wake region of the blade chord. The affects of the reversed flow are expended outside the propeller disk into the freestream region, about $X/R = 1.2$.

The significant three-dimensional feature of the flowfield wake, especially near the hub and the tip-blade regions, made the two-dimensional hypothesis of the vortex theories unsatisfactory.

References

[1]Wilson, R. E., "Wind-Turbine Aerodynamics," *Journal of Industrial Aerodynamics*, Vol. 5, 1980, pp. 357–372.

[2]Chang, L. K., and Sullivan, P., "Optimization of Propeller Blade Twist by an Analytical Method," *AIAA Journal*, Vol. 22, No. 2, 1984, pp. 252–255.

[3]Kobayakawa, M., and Onuma, H., "Propeller Aerodynamic Performance by Vortex-Lattice Method," *Journal of Aircraft*, Vol. 22, No. 8, 1985, pp. 649–654.

[4]Matsuo, Y., Arakawa, C., Saito, S., and Kobayashi, H., "Navier-Stokes Simulations of Flows Around a High-Speed Propeller," *Proceedings of the 3rd International Symposium on Computational Fluid Dynamics*, Nagoya, Japan, 1991, pp. 523–529.

[5]Poling, D., Dadone, L., and Telionis, D. P., "Blade-Vortex Interaction," *AIAA Journal*, Vol. 27, No. 6, 1989, pp. 694–699.

[6]Lee, D. J., and Smith, C. A., "Effect of Vortex Core Distortion on Blade-Vortex Interaction," *AIAA Journal*, Vol. 29, No. 9, 1991, pp. 1355–1362.

[7]George, V. V., Gaonkar, G. H., Prasad, J. V. R., and Schrage, D. P., "Adequacy of Modeling Turbulence and Related Effects on Helicopter Response," *AIAA Journal*, Vol. 30, No. 6, 1992, pp. 1468–1479.

[8]Lepicovsky, J., and Bell, W. A., "Aerodynamic Measurements About a Rotating Propeller with a Laser Velocimeter," *Journal of Aircraft*, Vol. 21, No. 4, 1984, pp. 264–271.

[9]Lepicovsky, J., "Laser Velocimeter Measurements in a Model Propeller Flowfield," *Journal of Fluids Engineering*, Vol. 110, Dec. 1988, pp. 350–354.

[10]Murthy, K. N. S., and Lakshminarayana, B., "Laser Doppler Velocimeter Measurements in the Tip Region of a Compressor Rotor," AIAA Paper 84-1602, June 1984.

[11]Favier, D., Rebont, J., and Maresca, C., "An Experimental Study of Three-Dimensional Characteristics of Propeller Wakes Under Stalling Conditions," *Journal of Fluids Engineering*, Vol. 99, Dec. 1977, pp. 745–752.

[12]Kotb, M. A., and Schetz, J. A., "Measurements of Three-Dimensional Turbulent Flow Behind a Propeller in a Shear Flow," *AIAA Journal*, Vol. 24, No. 4, 1986, pp. 570–577.

[13]Shekarriz, A., Fu, T. C., Katz, J., and Huang, T. T., "Near-Field Behavior of a Tip Vortex," *AIAA Journal*, Vol. 31, No. 1, 1993, pp. 112–117.

[14]Doebelin, E. O., *Measurement Systems Application and Design*, 3rd ed., McGraw–Hill, New York, 1883.